PHYSICAL REVIEW B VOLUME 15, NUMBER 11 1 JUNE 1977

Quadrupole interaction and static Jahn-Teller effect in the EPR spectra of Ir^{2+} in MgO and CaO

A. Raizman* and J. T. Suss
Solid State Physics Department, Israel Atomic Energy Commission, Soreq Nuclear Research Center, Yavne, Israel

W. Low
Microwave Division, The Racah Institute of Physics, The Hebrew University, Jerusalem, Israel
(Received 19 May 1975)

The electron-paramagnetic-resonance spectra of Ir^{2+} were studied in single crystals of MgO and CaO at X-band frequencies. The spectra exhibit a strong quadrupole interaction and a static Jahn-Teller effect. The electric field gradient required for the quadrupole interaction is caused here by Jahn-Teller distortions. At high temperatures the spectrum is isotropic, at low temperatures it consists of a superposition of three tetragonal spectra. The unusually high transition temperatures ($T_t > 120$ K) at which the transitions from the high-temperature to the low-temperature spectra occur, are consistent with a strong Jahn-Teller coupling. It could be concluded for both hosts that $\bar{\delta}/3\Gamma > 10$ and that the first excited vibronic level is a singlet A_1. The quadrupole interaction was found to be much larger than the hyperfine interaction in MgO ($Q/A_\perp \sim 2$) and smaller in CaO ($Q/A_\perp \sim 0.25$). The anomalous effects in the EPR spectra caused by the strong quadrupole interaction were interpreted by an exact diagonalization of the spin Hamiltonian using a FORTRAN IV version of the MAGNSPEC program.

I. INTRODUCTION

Electron-paramagnetic-resonance (EPR) spectra are usually characterized by a predominant Zeeman effect with the perturbation caused by the hyperfine interaction. Quadrupole interaction (QI) is usually much smaller than hyperfine interaction, not significantly affecting the EPR spectra, and the interpretation can be made by the usual perturbation-theory formulas.[1] We report here some unusual spectra in which the QI is large and these formulas are not applicable. An exact diagonalization of the spin Hamiltonian is necessary for the interpretation. This large quadrupole interaction was found in single crystals of MgO and CaO containing Ir^{2+} isotopes. The two isotopes ^{191}Ir and ^{193}Ir were expected to exhibit such an effect since they have large quadrupole moments and relatively small nuclear moments. In the EPR spectrum of Ir^{2+} in MgO we have found that the QI is even stronger than the hyperfine interaction. A strong quadrupole interaction of Ir^{2+} was observed[2] in the $Ir(CN)_5$ complex in KCl. Other possible isotopes which may be expected to exhibit strong QI are ^{197}Au, with a reported EPR spectrum in the Au(II) diethyldithiocarbonate complex,[3] and ^{155}Gd and ^{157}Gd with a reported strong QI in YPO_4.[4] In chabazite the QI of Cu^{2+} was found.[5]

The Ir^{2+} ions substitute for the cations in the fcc MgO and CaO lattice and are surrounded by an octahedron of six O^{2-} ions. The ground state of the Ir^{2+} ($5d^7$) low-spin ion in an octahedral crystal field is an orbital doublet ^2E ($t_{2g}^6 e_g$) undergoing a static Jahn-Teller (JT) effect. Thus the electric field gradient required for the QI is in our case caused by the JT distortions. A QI in a static JT-effect case was reported in the EPR spectrum of Cu^{2+} in NaCl.[6] A weak QI in systems exhibiting a dynamic JT effect was studied in the EPR spectra of La^{2+} and Sc^{2+}.[7,8] While in all cases reported so far the QI in JT ions was smaller than the hyperfine interaction, in the case of Ir^{2+} in MgO it is much larger.

II. EXPERIMENTAL

Single crystals of MgO doped with 0.5-mole% $IrCl_4$ were grown by the flux evaporation method from PbF_2.[9] Single crystals of CaO doped with Ir were grown for us by W.&C. Spicer Ltd., by melting $CaCO_3$ with 0.2-mole% Ir metal powder in an electric arc furnace. Spectrochemical analysis showed a concentration of the order of 1000 and 100 ppm of Ir in the MgO and CaO crystals, respectively. The as-grown MgO crystals were yellow in color; the as-grown CaO crystals were milky and slightly yellowish. No EPR spectrum which could be associated with Ir^{2+} ions was detected in the as-grown crystals.

After γ or x-ray irradiation the spectra of Ir^{2+} together with other Ir species were observed. These spectra are stable for many months in crystals kept in darkness and at room temperature. A weak Ir^{2+} spectrum was also produced by reducing the crystals at 1000 °C in hydrogen. In this case no other Ir spectra were observed. A VARIAN X-band EPR spectrometer was used

in the temperature range 4.2–300 K. The fitting of the spin Hamiltonian parameters to the EPR spectrum was carried out with an IBM 370/160 computer using the FORTRAN IV version of the MAGNSPEC program.[10]

III. THEORY

Ions possessing orbitally degenerate electronic ground states are subject to the JT effect. This effect has been studied extensively[1,8,11-14] and continues to be of interest. The vibronic Hamiltonian which represents the coupling between the orbital doublet $^2E_g(\theta, \epsilon)$ and the Q_θ and Q_ϵ modes of vibration is given by $\mathcal{H}_V = \mathcal{H}_0 + \mathcal{H}_{JT} + \mathcal{H}_W$. $\mathcal{H}_0$ includes the energy E_0 of the ^2E_g electronic state in the absence of vibronic coupling, the kinetic energy, and the elastic energy of the vibrational modes. $\mathcal{H}_{JT}$ and $\mathcal{H}_W$ describe the linear and nonlinear JT couplings, respectively. The JT stabilization energy E_{JT} obtained for the linear JT coupling is $E_{JT} = V^2/2\mu\omega^2$. E_{JT} corresponds to the equilibrium value $\rho = \rho_0 = |V|/\mu\omega^2$. V is the linear JT coupling coefficient. μ, ω, and ρ are the reduced mass, the angular frequency, and the radial coordinate of the vibrational modes. The ground state of $\mathcal{H}_V$ is a vibronic doublet E state, and with only linear JT coupling the first excited state is an accidentally degenerate doublet $(A_1 + A_2)$ with an energy above the ground state given (for $E_{JT}/\hbar\omega \gtrsim 1$) by $\Delta_1 = 2\alpha$, where $\alpha = \hbar\omega(4E_{JT}/\hbar\omega)^{-1}$. The nonlinear term of the vibronic Hamiltonian $\mathcal{H}_W$ yields three wells in the lower potential surface with a well barrier height of 2β, where β is the nonlinear JT coupling coefficient. In this case the excited doublet $(A_1 + A_2)$ is split and the lower singlet approaches the ground state asymptotically as β increases. The splitting between the ground doublet and the first excited singlet is called the tunneling splitting 3Γ and is inversely dependent on β. The lower excited state is A_1 if V and β have the same sign and A_2 if V and β are of opposite sign. Random strain with tetragonal symmetry will split the vibronic doublet E into two singlets with an energy separation δ. For 3Γ small enough, random strain can also cause an admixture of the excited singlet A_1 (or A_2) into one of the components of the strain split doublet.

The nature of the low-temperature EPR spectrum of a JT system is determined by the ratio $\bar{\delta}/3\Gamma$, where $\bar{\delta}$ is the mean random strain splitting of the doublet E. For small values of $\bar{\delta}/3\Gamma$ ($\bar{\delta}/3\Gamma < 0.1$) a dynamic JT effect is obtained. The lower doublet is treated as an isolated strain split doublet, and two EPR transitions of cubic anisotropy are observed. A value of $\bar{\delta}/3\Gamma > 5$ gives a static JT effect. In this case the random strain admixes the first excited singlet into the ground doublet. Each state of the effective triplet represents a distortion of the octahedron along the z, x, or y direction of the cubic axes. For this case the EPR spectrum consists of a superposition of three tetragonal spectra. For values of 3Γ comparable with $\bar{\delta}$ one gets an intermediate JT effect. The excited singlet A_1 (or A_2) is only partially admixed into the ground doublet. This feature demonstrates itself in the angular dependence and in the line shapes of the resonance lines.

A transition to an isotropic spectrum should be observed as the temperature is raised. There are two kinds of isotropic spectra: one is due to an excited vibronic singlet which is low enough to be populated, the other is due to relaxation processes causing a motional averaging of the anisotropic spectrum. The transition of the anisotropic to the isotropic spectrum is not sharp and both spectra can coexist over an appreciable temperature range.

We are concerned here with a static JT effect in which the tunneling splitting 3Γ is small compared with $\bar{\delta}$. For a d^7 low-spin configuration and an elongated octahedron the vibronic states of the effective ground triplet are:

$$Z = (3z^2 - r^2)\chi_z, \quad X = (3x^2 - r^2)\chi_x, \quad Y = (3y^2 - r^2)\chi_y,$$

where $(3z^2 - r^2)$ is the electronic part and χ_z is the vibrational part of the vibronic wave function Z, etc. (We discuss only the E_θ component of the electronic doublet, since our experimental results give $g_\perp > g_\parallel$, as shown in Table I.) This triplet is further split by random strains. If the strain is for example in the z direction, the Z state becomes the ground state at $-\delta + \Gamma$, and the other two levels of the triplet are located at $+\frac{1}{2}\delta$ and $+\frac{1}{2}\delta + 2\Gamma$. Because of the random character of the strains, the population of the different ground states X, Y, and Z is the same. Following Ham's treatment,[12] one gets the following spin Hamiltonain for the Z ground state:

$$\mathcal{H} = g_1\mu_B\vec{H}\cdot\vec{S} - qg_2\mu_B(3H_zI_z - \vec{H}\cdot\vec{S}) + A_1\vec{I}\cdot\vec{S} - qA_2(3I_zS_z - \vec{I}\cdot\vec{S}) - qQ'(3I_z^2 - \vec{I}\cdot\vec{I}) + \mu_N\vec{H}\cdot\vec{I}, \quad (1)$$

or in a more convenient form

$$\mathcal{H} = g_\parallel\mu_BH_zS_z + g_\perp\mu_B(H_xS_x + H_yS_y) + A_\parallel I_zS_z + A_\perp(I_xS_x + I_yS_y) + Q[I_z^2 - \tfrac{1}{3}I(I+1)] + \mu_N(H_zI_z + H_xI_x + H_yI_y). \quad (2)$$

Here g_1 and g_2, A_1 and A_2 are the isotropic and anisotropic parts of the g factor and of the hyperfine constant, respectively. μ_N is the nuclear magneton, μ_B is the Bohr magneton, q is the

reduction factor (for a strong JT coupling, $q=\frac{1}{2}$), and Q' is the quadrupole parameter. The resonance parameters of Eqs. (1) and (2) are related in the following way:

$$g_{\parallel}=g_1-2qg_2,\quad g_{\perp}=g_1+qg_2,$$
$$A_{\parallel}=A_1-2qA_2,\quad A_{\perp}=A_1+qA_2, \tag{3}$$
$$Q=-3qQ'.$$

The spin-Hamiltonian parameters can be obtained from crystalline-field-theory calculations to the first order of ζ, using the complementary hole scheme configurations $\bar{e}_g^3$ and $\bar{t}_{2g}\bar{e}_g^2$ instead of the ground and excited electronic configurations $t_{2g}^6 e_g^1$ and $t_{2g}^5 e_g^2$, respectively. Using the technique described by Sugano *et al.*,[15] we built the wave functions of the $\bar{t}_{2g}\bar{e}_g^2$ terms for octahedral symmetry (in order of increasing energy) $^4T_1(^3A_2)$, $^2T_1(^3A_2)$, $^2T_2(^1E)$, $^2T_1(^1E)$, and $^2T_2(^1A_1)$. The terms in parenthesis are due to the direct product $e_g\otimes e_g$. The separation between the ground state and the respective excited energy levels are designated as Δ_i ($i=1, 2, 3, 4, 5$). The following results were obtained for the Hamiltonian parameters by evaluating the corresponding matrix elements within the perturbed ground states ψ_θ^+ and ψ_θ^- obtained by mixing the ground and excited states via spin-orbit coupling:

$$g_{\parallel}=g_e-4k_{\pi\sigma}\zeta_{\pi\sigma}\left(\frac{1}{\Delta_2}-\frac{1}{\Delta_4}\right),$$
$$g_{\perp}=g_e+k_{\pi\sigma}\zeta_{\pi\sigma}\left(-\frac{1}{\Delta_2}+\frac{1}{\Delta_4}+\frac{3}{\Delta_3}+\frac{3}{\Delta_5}\right), \tag{4}$$

where $k_{\pi\sigma}$ is the orbital reduction factor defined as

$$k_{\pi\sigma}=\langle\tilde{t}_{2g}|\,L|\tilde{e}_g\rangle/\langle t_{2g}|\,L|e_g\rangle$$

(t_{2g} and e_g are pure d orbitals and $\tilde{t}_{2g}$ and $\tilde{e}_g$ are the corresponding molecular orbitals). $\zeta_{\pi\sigma}$ is the spin-orbit coupling between $\tilde{t}_{2g}$ and $\tilde{e}_g$ orbitals for an electron. g_e is the free-electron g factor.

$$A_{\parallel}=P\left[\frac{N_\pi N_\sigma}{k_{\pi\sigma}}g_{L\parallel}-\kappa+\tfrac{4}{7}N_\sigma^2+\tfrac{2}{7}N_\pi N_\sigma\zeta_{\pi\sigma}\left(-\frac{2}{\Delta_1}+\frac{1}{2\Delta_2}-\frac{3}{2\Delta_3}-\frac{3}{2\Delta_4}+\frac{3}{2\Delta_5}\right)\right],$$
$$A_{\perp}=P\left[\frac{N_\pi N_\sigma}{k_{\pi\sigma}}g_{L\perp}-\kappa-\tfrac{2}{7}N_\sigma^2-\tfrac{1}{7}N_\pi N_\sigma\zeta_{\pi\sigma}\left(-\frac{2}{\Delta_1}+\frac{1}{2\Delta_2}-\frac{3}{2\Delta_3}-\frac{3}{2\Delta_4}+\frac{3}{2\Delta_5}\right)\right]. \tag{5}$$
$$Q=-\tfrac{1}{7}e^2Q_0N_\sigma^2(1-R)\langle r^{-3}\rangle,$$

$P=2\gamma_N\mu_B\mu_N\langle r^{-3}\rangle$, N_σ, and N_π are the coefficients of the e_g and t_{2g} functions in the molecular orbitals $\tilde{e}_g$ and $\tilde{t}_{2g}$, respectively. κ is the core polarization factor, containing the effect of covalent bonding. γ_N is the nuclear magnetogyric ratio. $g_{L\parallel}$ and $g_{L\perp}$ are $g_{\parallel}-g_e$ and $g_{\perp}-g_e$, respectively. The expression for Q here contains only the contribution of the valence electrons to the electric field gradient. Q_0 is the nuclear electric quadrupole moment and $(1-R)$ is the Sternheimer shielding factor.

IV. RESULTS

The two stable isotopes ^{191}Ir and ^{193}Ir have, respectively, a natural abundance of 38.5% and 61.5% and nuclear magnetic moments of $(0.1453\pm0.0006)\mu_N$ and $(0.1583\pm0.0006)\mu_N$.[16] Both isotopes have a nuclear spin $I=\frac{3}{2}$. The ratio of the nuclear electric quadrupole moments $Q_0(^{193}\mathrm{Ir})/Q_0(^{191}\mathrm{Ir})$ of the two Ir isotopes is equal to 0.91 ± 0.03.[2] $Q_0(^{191}\mathrm{Ir})$ is about 0.9 b and $Q_0(^{193}\mathrm{Ir})$ is about 0.82 b.[17] The measured and calculated resonance parameters of Ir^{2+} in single crystals of MgO and CaO are summarized in Table I. The values of Q were obtained by exact diagonalization of the spin Hamiltonian using the MAGNSPEC program.[10]

In both crystals at low temperatures the EPR spectrum of Ir^{2+} consists of a superposition of three tetragonal spectra (due to the three different distorted sites) characteristic of a static JT effect. The principal symmetry axes of the tetragonal spectra are the [100]-type crystal axes. The spectra at $g_{\parallel}$ (Figs. 1 and 2) consist of a four-line equally spaced characteristic spectrum ($I=\frac{3}{2}$) for each isotope due to $\Delta m=0$ transitions. More complicated spectra are observed at $g_{\perp}$ (Figs. 3 and 4). The spectrum at $g_{\perp}$ in CaO (Fig. 3) exhibits features close to those expected for an ion with $S=\frac{1}{2}$, $I=\frac{3}{2}$, and a nonzero value of Q, as obtained from second-order perturbation theory.[1] The lower intensity lines are due to $\Delta m=\pm2$ transitions. A careful examination of the spectrum shows deviation from the features expected from perturbation theory in the form of slightly unequal spacing of the hyperfine lines due to $\Delta m=0$ transitions. Further, an asymmetrical spacing of the lines due to $\Delta m=\pm2$ transitions about the two $\Delta m=0$ inner lines is not consistent with perturbation-theory predictions. In MgO a drastic change is observed in the nature of the spectrum at $g_{\perp}$ (Fig. 4). Figure 5 shows the spectrum in MgO with H_{dc} along a [110] direction at $g_{[110]}$, and Fig. 6 with H_{dc} at $\Theta=23°$ (the

TABLE I. Resonance parameters for Ir^{2+} in single crystals of CaO and MgO.

Host	g	$A[10^{-4}\ cm^{-1}]$	$Q[10^{-4}\ cm^{-1}]$	$Q/A_\perp$	$T[K]$
CaO [a]	$g_\parallel = 1.9517(5)$	$A_\parallel(^{191}Ir) = 32.6(1.0)$ $A_\parallel(^{193}Ir) = 35.5(1.0)$	$Q(^{191}Ir) = 15.0(1.0)$ $Q(^{193}Ir) = 13.7(1.0)$		93
	$g_\perp = 2.6814(5)$	$A_\perp(^{191}Ir) = 50.8(1.0)$ $A_\perp(^{193}Ir) = 55.3(1.0)$		$(Q/A_\perp)(^{191}Ir) = 0.295$ $(Q/A_\perp)(^{193}Ir) = 0.248$	93
	$\frac{1}{3}(g_\parallel + 2g_\perp) = 2.438$ $[\frac{1}{3}(g_\parallel^2 + 2g_\perp^2)]^{1/2} = 2.462$	$\bar{A}_{[111]}(^{191}Ir) = 44.7$, [b] $\bar{A}_{[111]}(^{193}Ir) = 48.7$ [b] $A_{[111]}(^{191}Ir) = 47.6$, [b] $A_{[111]}(^{193}Ir) = 51.7$ [b]			
	$g_{isotropic} = 2.467(5)$	$A_{isotropic} = 47.0(2.0)$			233
MgO	$g_\parallel = 1.978(1)$	$A_\parallel(^{191}Ir) = 5.5(5)$ $A_\parallel(^{193}Ir) = 6.0(5)$	$Q(^{191}Ir) = 32.2(5)$ $Q(^{193}Ir) = 29.2(5)$		4.2
	$g_\perp = 2.464(1)$	$A_\perp(^{191}Ir) = 14.7(5)$ $A_\perp(^{193}Ir) = 16.1(5)$		$(Q/A_\perp)(^{191}Ir) = 2.190$ $(Q/A_\perp)(^{193}Ir) = 1.814$	4.2
	$\frac{1}{3}(g_\parallel + 2g_\perp) = 2.302$ $[\frac{1}{3}(g_\parallel^2 + 2g_\perp^2)]^{1/2} = 2.313$	$\bar{A}_{[111]}(^{191}Ir) = 11.6$, [b] $\bar{A}_{[111]}(^{193}Ir) = 12.7$ [b] $A_{[111]}(^{191}Ir) = 13.0$, [b] $A_{[111]}(^{193}Ir) = 14.3$ [b]			
	$g_{isotropic} = 2.309(5)$	Not resolved			273

[a] A preliminary account of the work on Ir^{2+} in CaO was presented in J. T. Suss and A. Raizman, Bull. Am. Phys. Soc. 20, 807 (1975).

[b] $\bar{A}_{[111]}$ and $A_{[111]}$ were calculated as $\bar{A}_{[111]} = \frac{1}{3}(A_\parallel + 2A_\perp)$ and $A_{[111]} = (1/g_{[111]})[\frac{1}{3}(g_\parallel^2 A_\parallel^2 + 2g_\perp^2 A_\perp^2)]^{1/2}$ respectively.

angle Θ is measured with respect to the axis of distortion). Figure 7 shows the spectrum in CaO with H_{dc} along a [110] direction at $g_{[110]}$. The linewidths of the low-temperature spectra in both crystals were very narrow. The narrowest observed peak-to-peak linewidths of the first derivatives of the absorption lines at $g_\parallel$ and $g_\perp$ were about 1 G. The symmetrical line shapes do not exhibit any distortions which could indicate a deviation from the "pure" static JT effect. This situation of very little (or no) overlap between

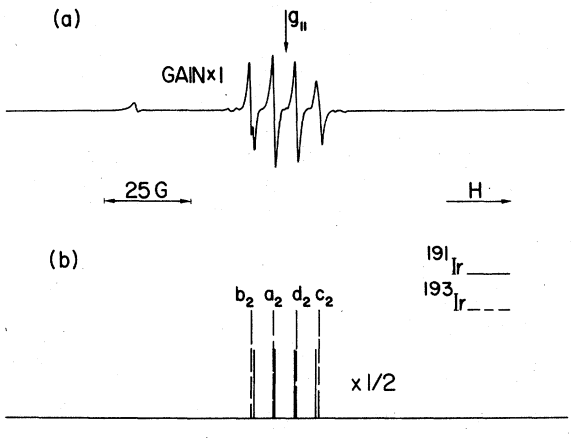

FIG. 1. (a) EPR spectrum of Ir^{2+} in a single crystal of MgO at $g_\parallel$, 4.2 K, 9.433 GHz, and a microwave power of 10 μW. H_{dc} is along a [100] direction. (b) The calculated spectrum. The intensities are multiplied by $\frac{1}{2}$ (Ref. 18).

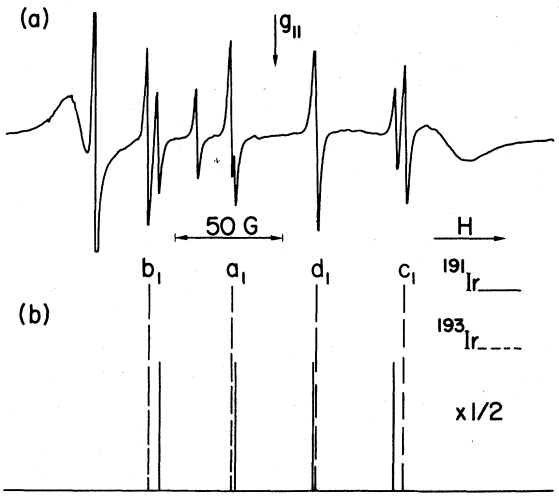

FIG. 2. (a) EPR spectrum of Ir^{2+} in a single crystal of CaO at $g_\parallel$, 93 K, 9.093 GHz, and a microwave power of 40 mW. H_{dc} is along a [100] direction. (b) The calculated spectrum. The intensities are multiplied by $\frac{1}{2}$.

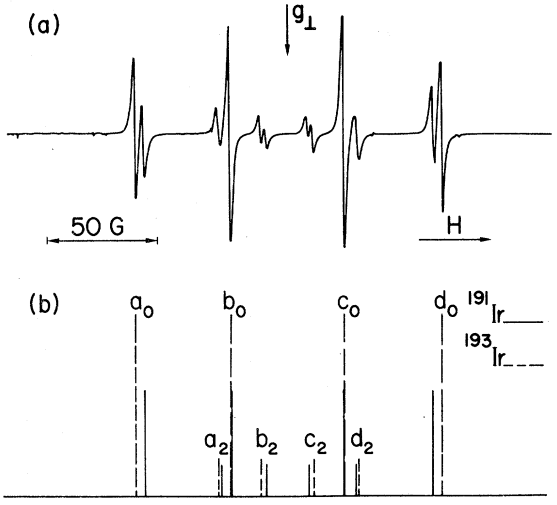

FIG. 3. (a) EPR spectrum of Ir^{2+} in a single crystal of CaO at $g_\perp$, 93 K, 9.093 GHz, and a microwave power of 40 mW. H_{dc} is along a [100] direction. (b) The calculated spectrum.

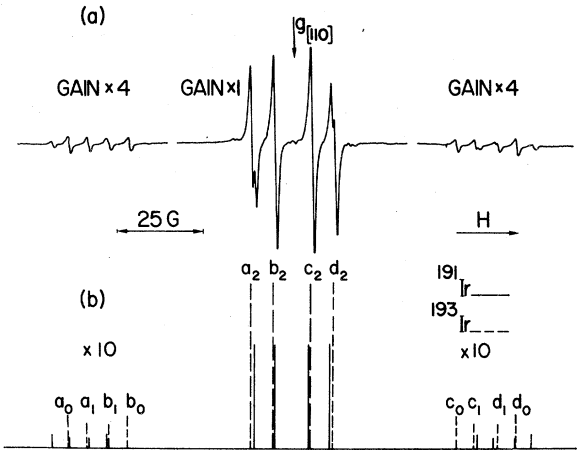

FIG. 5. (a) EPR spectrum of Ir^{2+} in a single crystal of MgO at $g_{[110]}$, 4.2 K, 9.433 GHz, and a microwave power of 10 μW. H_{dc} is along a [110] direction (two sites coincide). (b) The calculated spectrum. The intensities of the satellites are multiplied by 10.

strain-broadened EPR lines is further supported by the absence of the low-temperature isotropic spectrum.

The assignment of the spectra of the JT ions reported in this paper to Ir^{2+} is also supported by the results of the irradiation and thermal treatments. As pointed out in Sec. II the Ir^{2+} spectra can be produced in Ir-doped MgO and CaO crystals either by ionizing radiation or reduction in hydrogen. In MgO ionizing radiation produces Ir^{4+},[19,20] in addition to Ir^{2+}. In the as-grown CaO crystals, (grown in an electric arc furnace) Ir^{4+} species were also observed,[20] which is not surprising considering the strong oxidizing atmosphere during growth. Heating of the crystals at 1000 °C in an oxygen atmosphere did not produce any of the Ir^{2+} species. It seems that most of the Ir is present in the as-grown crystals as Ir^{3+}, which is converted to Ir^{2+} by trapping an electron during either irradiation or reduction.

The interpretation of the spectra could not be made in the conventional way by solving the spin Hamiltonian using second-order perturbation

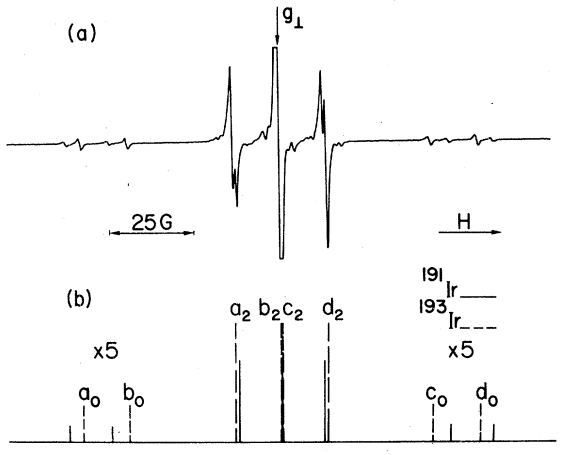

FIG. 4. (a) EPR spectrum of Ir^{2+} in a single crystal of MgO at $g_\perp$, 4.2 K, 9.433 GHz, and a microwave power of 10 μW. H_{dc} is along a [100] direction. (b) The calculated spectrum. The intensities of the satellites (designated as lines a_0, b_0, c_0, and d_0) are multiplied by 5.

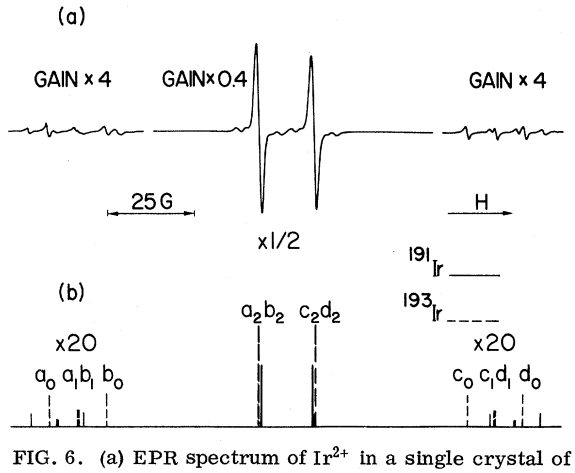

FIG. 6. (a) EPR spectrum of Ir^{2+} in a single crystal of MgO at $\Theta = 23°$, 4.2 K, 9.433 GHz, and a microwave power of 100 μW. At this angle a partial collapsing of the spectrum occurs, as shown also in Fig. 9. (b) The calculated spectrum. The intensities of the main spectrum are multiplied by $\frac{1}{2}$, the intensities of the satellites are multiplied by 20.

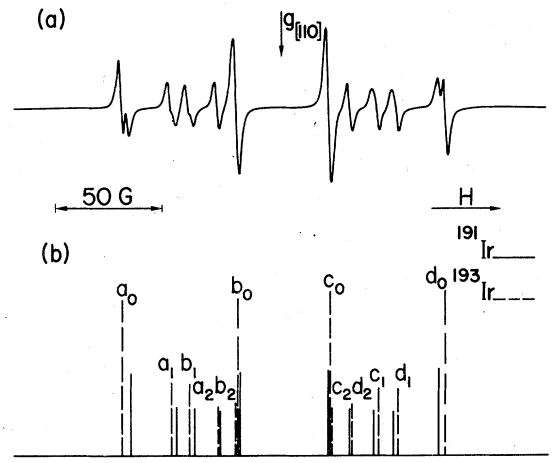

FIG. 7. (a) EPR spectrum of Ir^{2+} in a single crystal of CaO at $g_{[110]}$, 93 K, 9.093 GHz, and a microwave power of 40 mW. H_{dc} is along a [110] direction. (b) The calculated spectrum.

theory.[1] While at $g_\parallel$ the effects of QI vanish, at $g_\perp$ a large QI had to be taken into account, which necessitated modification of the conventional perturbation theory. An 8×8 matrix resulting from $|S=\frac{1}{2}, I=\frac{3}{2}\rangle$ had to be diagonalized. The problem was simplified by using the transformed spin Hamiltonian[1] (neglecting the nuclear Zeeman interaction)

$$\mathcal{H}=\mathcal{H}_Z+\mathcal{H}_{hf}+\mathcal{H}_Q,$$

where

$$\mathcal{H}_Z=g\mu_B H S_z, \tag{6}$$

$$\mathcal{H}_{hf}=AS_zI_z+\frac{A_\parallel A_\perp}{A}S_xI_x + \frac{A_\perp^2-A_\parallel^2}{A}\frac{g_\parallel g_\perp}{g^2}\sin\Theta\cos\Theta S_xI_z+A_\perp S_yI_y, \tag{7}$$

$$\mathcal{H}_Q=\tfrac{1}{2}Q[I_z^2-\tfrac{1}{3}I(I+1)](3\cos^2\psi-1) - Q(I_xI_z+I_zI_x)\cos\psi\sin\psi+\tfrac{1}{2}Q(I_x^2-I_y^2)\sin^2\psi, \tag{8}$$

where

$$g=(g_\parallel^2\cos^2\Theta+g_\perp^2\sin^2\Theta)^{1/2},$$
$$A=(g_\parallel^2A_\parallel^2\cos^2\Theta+g_\perp^2A_\perp^2\sin^2\Theta)^{1/2}/g, \tag{9}$$
$$\sin\psi=\frac{g_\perp A_\perp}{gA}\sin\Theta,\quad \cos\psi=\frac{g_\parallel A_\parallel}{gA}\cos\Theta.$$

Θ is the angle between the z direction and the applied magnetic field H_{dc}.

If one negelcts the off-diagonal elements of $\mathcal{H}_{hf}$ in Eq. (7), the 8×8 matrix is reduced to a block diagonal of two 4×4 matrices, one with $S_Z=\frac{1}{2}$ and the other with $S_Z=-\frac{1}{2}$. Since $\mathcal{H}_Z$ is already diagonal and proportional to the unit matrix in each block, the diagonalization of $(1/g\mu_B)(\mathcal{H}_{hf}+\mathcal{H}_Q)$ gives the relative positions of the resonance fields with respect to H_0 (where $H_0=h\nu/g\mu_B$). For $\Theta=0$, the matrices are diagonal and the quadrupole interaction ($\mathcal{H}_Q$) has no effect on the hyperfine structure. For $\Theta=90°$, the 4×4 matrices are further reduced to two 2×2 matrices, which can be solved analytically. From this solution the positions and intensities of the eight resonance lines are obtained as follows:

(i) A group of four lines, which we designate as group [0] (due to the four possible combinations of the "+" and "−" signs) with intensities

$$I_{[0]}\propto|\sin(\alpha^+-\alpha^-)|^2, \tag{10}$$

at fields given by

$$g_\perp\mu_B(H-H_0)=\mp(A_\perp/2)\mp(C+D). \tag{11}$$

(ii) Another group of four lines, which we designate as group [2], with intensities

$$I_{[2]}\propto|\cos(\alpha^+-\alpha^-)|^2, \tag{12}$$

at fields given by

$$g_\perp\mu_B(H-H_0)=\mp(A_\perp/2)\mp(C-D), \tag{13}$$

where

$$C=(A_\perp^2+2A_\perp Q+4Q^2)^{1/2},$$
$$D=(A_\perp^2-2A_\perp Q+4Q^2)^{1/2},$$
$$\tan2\alpha^\pm=\sqrt{3}\,Q/(\pm A_\perp-Q), \tag{14}$$

here

$$H_0=h\nu/g_\perp\mu_B.$$

The calculated positions and intensities of the eight resonance lines for $\Theta=90°$ from the above equations are shown in Fig. 8. From this figure it can be seen that for small values of $Q/A_\perp$ one obtains a group of four strong ("allowed") lines due to the $\Delta m=0$ transitions (group [0], designated a_0, b_0, c_0, and d_0) and a group of four weak ("forbidden") lines due to $\Delta m=\pm2$ transitions (group [2], designated a_2, b_2, c_2, and d_2). The designation of the resonance lines is consistent with Ref. 1. When $Q/A_\perp$ increases, the intensity of group [0] decreases and that of group [2] increases. At $Q/A_\perp=0.5$ the intensities of both groups are equal. It is also of interest to note that at this point there is a crossing of the two inner lines of group [0] (lines b_0 and c_0) with the two outer lines of group [2] (lines a_2 and d_2). The assignment "allowed" and "forbidden," of course, does not have the usual meaning here because of the strong admixture of the wave functions with different m values. For values of $Q/A_\perp>0.5$, the intensity of group [0] becomes smaller than that of group [2]. Further, for values of $Q/A_\perp>1$,

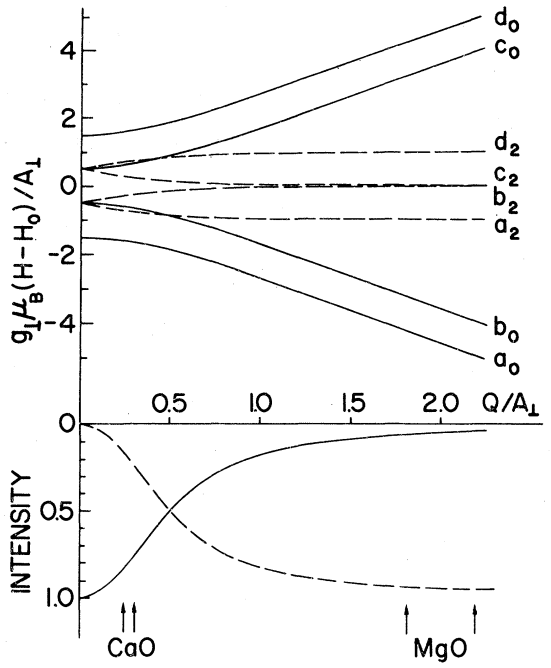

FIG. 8. Calculated positions and intensities of the resonance lines versus $Q/A_\perp$ at $g_\perp$ for a general case of $S=\frac{1}{2}$ and $I=\frac{3}{2}$. The ratios $(Q/A_\perp)(^{193}\mathrm{Ir})=1.814$ and $(Q/A_\perp)(^{191}\mathrm{Ir})=2.190$ for Ir^{2+} in MgO, and $(Q/A_\perp)(^{193}\mathrm{Ir})=0.248$ and $(Q/A_\perp)(^{191}\mathrm{Ir})=0.295$ in CaO are indicated by arrows. Solid line represents group [0], dashed line represents group [2].

the two inner lines of group [2] (lines b_2 and c_2) nearly coincide and the separation between the low-field doublet of group [0] (lines a_0 and b_0) and the high-field doublet of group [0] (lines c_0 and d_0) increases linearly with increasing $Q/A_\perp$. The separation between the lines a_0 and b_0, c_0 and d_0, a_2 and c_2, b_2 and d_2 is practically constant throughout the whole range of $Q/A_\perp$, and equal to 1 in units of $A_\perp$. In an arbitrary direction the total number of lines observed is 12. The four additional lines are usually referred to as transitions between $\Delta m=\pm 1$ (group [1], which we designate as a_1, b_1, c_1, and d_1), for small values of Q. The relative intensities of the different groups of lines are a strong function of the angle.

The EPR spectra of Ir^{2+} in CaO and MgO reported in this paper exhibit the following interesting unconventional features: (a) unusual positions of the resonance lines; (b) a variation in the relative intensities of the groups [0], [1], and [2]; and (c) the relative intensities of the lines due to the ^{193}Ir and ^{191}Ir isotopes are not preserved and vary from group to group. The spectra at $g_\perp$ shown in Figs. 3 and 4, for CaO and MgO, respectively, can be interpreted with the help of Fig. 8. The $Q/A_\perp$ ratios obtained from the measured spectrum at $g_\perp$ are indicated by two arrows for each crystal (CaO and MgO) in Fig. 8 and their values are given in Table I. For each host the arrows corresponding to the lower and higher $Q/A_\perp$ ratios belong to the ^{193}Ir and ^{191}Ir isotopes, respectively. The spectrum due to the isotope ^{193}Ir [broken lines in Figs. 3(b) and 4(b)] and due to the isotope ^{191}Ir [solid lines in Figs. 3(b) and 4(b)] each consist of two groups of lines: group [2] (designated a_2, b_2, c_2, d_2 in Fig. 8) and group [0] (designated a_0, b_0, c_0, d_0 in Fig. 8). In the case of CaO (Fig. 3), the dominant spectrum is due to group [0] as expected for values $Q/A_\perp < 0.5$ (see Fig. 8). In the case of MgO (Fig. 4), the dominant spectrum is due to group [2], with lines b_2 and c_2 coinciding (group [0] appears here as small satellites flanking group [2]), in accordance with the theoretical predictions for large $Q/A_\perp$ ratios, as seen in Fig. 8.

The deviations of the relative intensities of the spectra due to the two isotopes (in each group) from the ratio of their natural abundances stem from the different values of $Q/A_\perp$ for each isotope (see Fig. 8). This effect is more pronounced when the intensities of the group are weak. This can be seen clearly in group [2] for CaO (Fig. 3) and in group [0] for MgO (Fig. 4).

It was mentioned above that in an arbitrary direction the total number of lines due to each isotope is 12. Thus at $g_{[110]}$ (Figs. 5 and 7) an additional doublet (for each isotope), belonging to group [1], can be seen located symmetrically between the doublets a, b and c, d of group [0]. This feature is demonstrated clearly if one compares the spectra and the respective stick diagrams in Figs. 4 and 5 with those in Figs. 3 and 7 for MgO and CaO, respectively. The computer-calculated angular variation of the positions of the resonance lines, relative to H_0 (where $H_0=h\nu/g\mu_B$), is shown in Figs. 9 and 10, for MgO and CaO, respectively. For this calculation the parameters given in Table I were used. It was found that these calculated angular variations agree well with the experimentally observed positions of the resonance lines. It can be seen from Fig. 9 and 10 that there is a crossing of the resonance lines a_2 with b_2, and c_2 with d_2, in group [2], as well as a crossing of a_1 with b_1, and c_1 with d_1, in group [1], in the same vicinity. The angle at which the crossing occurs agrees with the theoretically predicted one for small values of $Q/A_\perp$: $\tan\Theta=\sqrt{2}\,(g_\parallel A_\parallel/g_\perp A_\perp)$.[1]

The angular variations of the computer-calculated relative intensities of the resonance lines of group [0] ($I_{[0]}$), group [1] ($I_{[1]}$), and group [2] ($I_{[2]}$) are shown in Figs. 11 and 12 for MgO

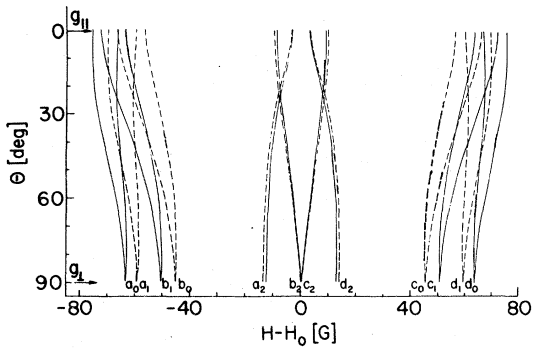

FIG. 9. Computer-calculated angular variation of the EPR spectrum of Ir^{2+} in a single crystal of MgO (one site only) relative to H_0. Θ is measured with respect to the axis of distortion. The solid and broken curves correspond to ^{191}Ir and ^{193}Ir, respectively.

and CaO, respectively. The experimentally observed intensities were in agreement with the theoretically calculated values. It should be noted that the designation of the groups was made at $g_{\perp}$, and is used throughout the angular variation of the lines. The amount of admixture of the wave functions with different m values changes during the angular variation, so that the four lines at $g_{\parallel}$, called group [2] in the case of MgO, and group [1] in the case of CaO, belong to transitions with $\Delta m = 0$.

As pointed out in Sec. III, the Ir^{2+} ion in MgO and CaO undergoes a static JT effect.

In MgO, in the temperature range 170–300 K, the spectrum consists of one isotropic wide line at $g_{\text{isotropic}} = 2.309 \pm 0.005$, as shown in Table I. This value is within the experimental error, equal to

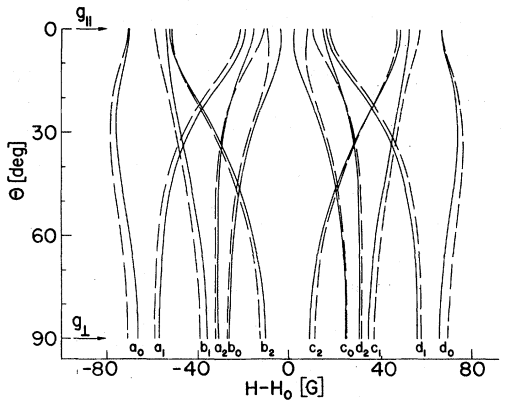

FIG. 10. Computer-calculated angular variation of the EPR spectrum of Ir^{2+} in a single crystal of CaO (one site only) relative to H_0. Θ is measured with respect to the axis of distortion. The solid and broken curves correspond to ^{191}Ir and ^{193}Ir, respectively.

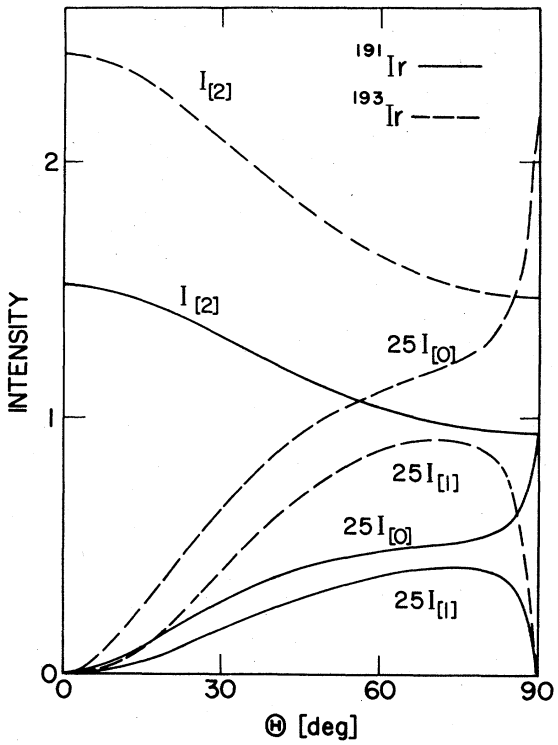

FIG. 11. The angular variation of the calculated relative intensities of the resonance lines of group [0] ($I_{[0]}$), group [1] ($I_{[1]}$), and group [2] ($I_{[2]}$) of Ir^{2+} in a single crystal of MgO. For each group the average value of the intensities of the four components is plotted. Θ is measured with respect to the axis of distortion.

the calculated

$$g_{[111]} = [\tfrac{1}{3}(g_{\parallel}^2 + 2g_{\perp}^2)]^{1/2}, \tag{15}$$

for a static JT effect. We have studied the linewidth in the temperature range 120–300 K and found the behavior in the [111] and [100] directions to differ. The peak-to-peak linewidth of the first derivative of the absorption line at 300 K is approximately 60 G. At this temperature, when H_{dc} is rotated in the (110) plane, the linewidth and intensity are unchanged. When the temperature is lowered below 300 K and H_{dc} is along a [111] direction, a gradual decrease in the linewidth is observed. In the [100] direction when the temperature is lowered a decrease in the linewidth is also observed, however to a lesser extent. In the vicinity of 190 K, the linewidth in the [100] direction has a minimum and below this temperature (in the same direction) it starts to increase, until at 150 K no line is detected. At 120 K a superposition of three tetragonal spectra replace the isotropic line. Thus in this case the transition from the isotropic to the anisotropic spectrum occurs in the temperature range 120–170 K.

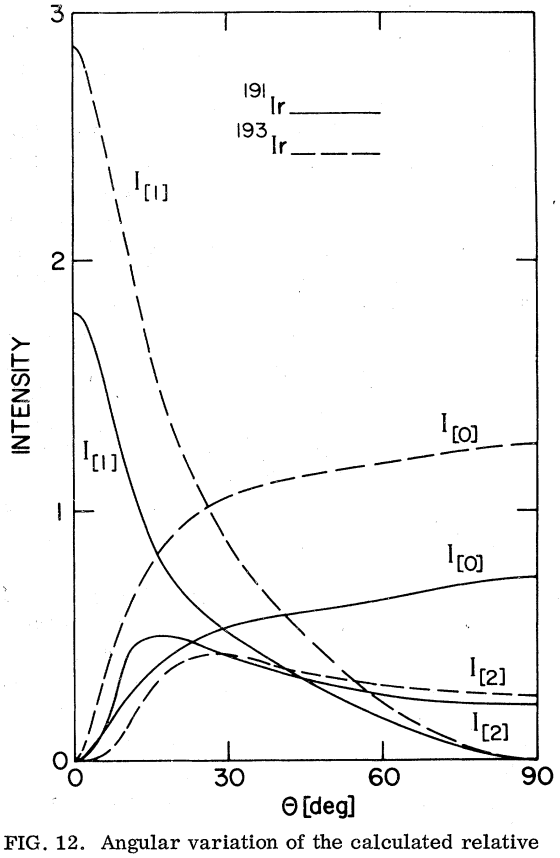

FIG. 12. Angular variation of the calculated relative intensities of the resonance lines of group [0] ($I_{[0]}$), group [1] ($I_{[1]}$), and group [2] ($I_{[2]}$) of Ir^{2+} in a single crystal of CaO. For each group the average value of the intensities of the four components is plotted. Θ is measured with respect to the axis of distortion.

In CaO, in the range 180–273 K, the spectrum consists of an isotropic quartet at $g_{\text{isotropic}} = 2.467 \pm 0.005$ with $A_{\text{isotropic}} = 47.0 \pm 2.0\ 10^{-4}\ \text{cm}^{-1}$, as shown in Table I. This $g_{\text{isotropic}}$ is also within experimental error of the calculated $g_{[111]}$ [Eq. (15)] of the static JT effect. The transition between the isotropic and anisotropic spectrum takes place here between 150–180 K. Below 150 K the spectrum consists of a superposition of three tetragonal spectra. The isotropic and anisotropic spectra of Ir^{2+} in CaO at 203 and 93 K with H_{dc} approximately along a [111] direction are shown in Fig. 13. The anisotropic spectrum is complicated due to the QI. In the isotropic spectrum the QI vanishes, as expected for effective cubic symmetry. The peak-to-peak linewidth of the first derivative of the absorption line at 203 K in the [111] direction is approximately 18 G. The high-temperature linewidth is anisotropic, however, it could not be studied in detail because of insufficient signal-to-noise ratio.

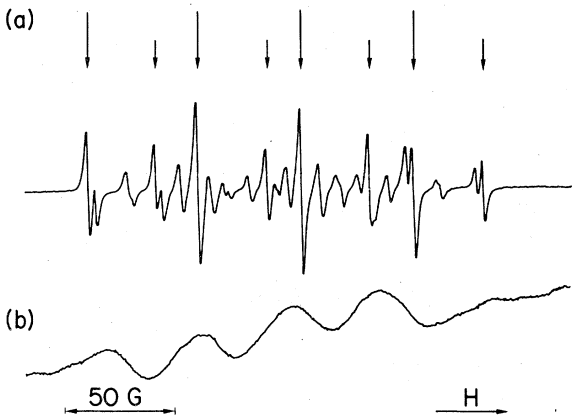

FIG. 13. EPR spectrum of Ir^{2+} in a single crystal of CaO, with H_{dc} approximately along a [111] direction at 9.112 GHz and a microwave power of 40 mW. (a) The anisotropic spectrum at 93 K, with gain ×1 and modulation ×1. The small arrows indicate the group [0] lines of one site and the large arrows indicate the other two coinciding sites of the same group. (b) The isotropic spectrum at 203 K, with gain ×3 and modulation ×10.

V. DISCUSSION

Inspection of the g factors given in Table I shows that (a) $g_{\parallel} < g_{\perp}$ for both crystals, (b) $g_{\parallel} < g_e$ for both crystals, (c) $g_{\parallel(\text{CaO})} < g_{\parallel(\text{MgO})}$, (d) $g_{\text{isotropic (CaO)}} > g_{\text{isotropic (MgO)}}$, (e) $g_{\perp(\text{CaO})} > g_{(\text{MgO})}$. We shall now discuss these points.

(a) The fact that $g_{\parallel} < g_{\perp}$ for the $^2E_g(t_{2g}^6 e_g)$ configuration indicates an elongated octahedron with a ground state E_θ, when the distortion of the octahedron is along the z direction. For this case the first excited singlet is A_1, and for a strong JT coupling ($q = \frac{1}{2}$), $g_{\parallel} = g_1 - g_2$ and $g_{\perp} = g_1 + \frac{1}{2}g_2$.

(b) $g_{\parallel} < g_e$ is consistent with Eq. (4), since $\Delta_2 < \Delta_4$. Values of $g_{\parallel}$ smaller than g_e were obtained also, e.g., for $Ir(CN)_5$ species[21] and the isoelectronic Pt^{3+} in MgO,[22] $BaTiO_3$,[23] YAlG,[24] and Al_2O_3.[25] On the other hand, for Rh^{2+} in MgO[26] and CaO,[27] and Ni^{3+} in MgO[28] and CaO,[29] it was found that $g_{\parallel} > g_e$. This positive g shift can be obtained by including the $(\zeta/\Delta_i)^2$ terms in Eq. (4). The main contribution will be from the term[30] $+2(\zeta/\Delta_1)^2$ which becomes appreciable near the crossover of the $^2E - {}^4T_1$ levels (at $Dq/B = 2.15$) of the Tanabe-Sugano diagram[31] for the d^7 configuration. For sufficiently large values of Dq/B, the term $2(\zeta/\Delta_1)^2$ can be neglected, which causes a negative g shift. Using values of $Dq \sim 2000\ \text{cm}^{-1}$ and $B \sim 300\ \text{cm}^{-1}$ obtained by extrapolation of data on Ir^{3+},[32] one gets $Dq/B \sim 6.6$, which is well beyond the crossover of the $^2E - {}^4T_1$ levels and explains the negative g shift obtained for Ir^{2+} in MgO and CaO. It should be emphasized that in the absence

of optical data on Ir^{2+} the above values (Dq and B) should be considered as rough estimates only.

(c) The larger negative g shift (of $g_{\parallel}$ from g_e) in CaO as compared with MgO is also consistent with Eq. (4). The cation-anion distance is 2.1 and 2.4 Å in MgO and CaO, respectively, and thus $\Delta_{(MgO)} > \Delta_{(CaO)}$.

(d) and (e) Using Eqs. (3) and (4), with $q = \frac{1}{2}$, and assuming (according to the Tanabe-Sugano diagram for our case) that $1/\Delta_2 \sim 1/\Delta_3$, and $1/\Delta_3 - 1/\Delta_4 \geq 0$ and small compared with $1/\Delta_2 + 1/\Delta_5$, one obtains

$$g_1 \sim g_e + 2k_{\pi\sigma}\zeta_{\pi\sigma}(1/\Delta_4 + 1/\Delta_5) > g_e ,$$
$$g_2 \sim 2k_{\pi\sigma}\zeta_{\pi\sigma}(1/\Delta_2 + 1/\Delta_5) > 0. \qquad (16)$$

Thus, $g_{1(MgO)} < g_{1(CaO)}$, $g_{2(MgO)} < g_{2(CaO)}$, and therefore, $g_{\perp(MgO)} < g_{\perp(CaO)}$. This is consistent with our results.

Inspection of the hyperfine structure constants given in Table I reveals that $A_{\perp} > A_{\parallel}$ for both crystals and $A_{[111](CaO)} > A_{[111](MgO)}$. It follows from simple considerations of $A_{\parallel}$, $A_{\perp}$, and $A_{isotropic}$ that $A_{\parallel}$ and $A_{\perp}$ must have the same sign, and therefore, according to Eq. (3), $|A_1| > |A_2|$, and since $A_{\perp} > A_{\parallel}$, A_1 and A_2 also have the same sign.

Let us consider, at least in a qualitative way, the core polarization contribution to the hyperfine splitting. (We shall refer here only to the isotope ^{193}Ir.) From Eqs. (3) and (5), one obtains for A_1

$$A_1 = P[\tfrac{1}{3}(N_{\pi}N_{\sigma}/k_{\pi\sigma})(g_{L\parallel} + 2g_{L\perp}) - \kappa]. \qquad (17)$$

The best fit between the measured and calculated spectra at $g_{\perp}$ was obtained for $Q/A_{\perp} < 0$. Choosing $Q < 0$ [Eq. (5)] one obtains $A_1 > 0$. Using $N_{\pi}N_{\sigma}/k_{\pi\sigma} = 1$ (for the estimation of κ we neglect here covalent bonding) and $\langle r^{-3} \rangle = 10.95$ a.u.,[33] for $A_1 > 0$, we obtain $\kappa = -0.07$ and -0.97, and $\chi = 1.1$ a.u. and 15.9 a.u. for MgO and CaO, respectively. Freeman *et al.*[34] calculated χ for divalent $5d$ ions and obtained values from -17 to -18 a.u. Our deviation from these calculated values of χ may be due to covalent effects and partial admixing of a $6s$ wave function which gives rise to a positive contribution to the isotropic hyperfine interaction. $\chi > 0$ was also found by Vugman *et al.* for Ir^{2+},[2] and for a few other d^7 ions.[35]

An estimation of N_{σ}^2 from Eq. (5), with $Q_0(^{193}Ir) = 0.82$ b,[17] $1 - R = 0.74$, and the measured values of $Q(^{193}Ir)$ (Table I), gives $N_{\sigma}^2 = 0.42$ and 0.20 for MgO and CaO, respectively. These small values of N_{σ}^2 indicate strong covalency as expected for a $5d$ ion. It is not reasonable that CaO should be more covalent than MgO. It is generally accepted that the electric field gradient on the metal ion of a complex is the sum of a valence electric field gradient and a contribution due to the lattice. Equation (5) takes into account only the valence

TABLE II. Vibronic parameters for Ir^{2+} in MgO and CaO.

		MgO	CaO
$\bar{\delta}/3\Gamma$		>10	>10
V_s	strain coupling coefficient (cm^{-1})	4.5×10^4	2.75×10^4
$\bar{\delta}$	mean random strain splitting (cm^{-1})	~4.5	~4.5
3Γ	tunneling splitting (cm^{-1})	< 0.45	< 0.45
V	linear JT coupling coefficent ($erg\,cm^{-1}$)	3.68×10^{-4}	1.93×10^{-4}
$\hbar\omega$	energy of the E_g mode vibration (cm^{-1})	400	300
E_{JT}	Jahn-Teller energy (cm^{-1})	2230	1140
ρ_0	equilibrium value of the radial coordinate ρ (Å)	0.237	0.235
$E_{JT}/\hbar\omega$		5.6	3.8
α	rotational kinetic energy (cm^{-1})	18	20
2β	height of barrier separating adjacent wells (cm^{-1}). (β is the nonlinear JT coupling coefficient.)	>740	>840
Δ	splitting between A_1 and A_2 (cm^{-1})	>280	>320
$\Delta\omega_L = 2\pi\nu(g_{\perp} - g_{\parallel})/g_{[111]}$ (sec^{-1})		12.5×10^9	17.5×10^9
τ	reorientation relaxation time (sec)	27×10^{-9}	14×10^{-9}
T_t	transition temperature at which the transition from low- to high-temperature spectrum occurs (K)	120–170	160–180

electric-field gradient. Therefore, a more detailed theory is needed to interpret our results for the quadrupole parameter.

Finally we wish to discuss the vibronic parameters summarized in Table II. As pointed out above, the first excited singlet in our case is A_1. Thus V and β, the linear and nonlinear JT coupling coefficients, respectively, are positive. The ratio $\bar{\delta}/3\Gamma$, estimated from the line shape and the angular dependence of the low-temperature spectrum, is greater than 10 for both crystals and defines our spectra as a "pure" static JT effect. The strain coupling coefficient V_s was calculated according to Ham,[12] and using $\langle r^2\rangle = 2.91$ a.u. and $\langle r^4\rangle = 14.66$ a.u.[33] The mean random strain splitting is defined[12] as $\bar{\delta} = 2qV_s(e_\theta^2 + e_\epsilon^2)^{1/2}$, where e_θ and e_ϵ are the θ and ϵ components of the strain tensor e, respectively. Stoneham[36] has shown from an analysis of EPR linewidths that typical residual strains of $\sim 2\times 10^{-4}$ are present at the sites of Fe^{2+} in MgO. Assuming that similar strains are present at a typical Ir^{2+} site in MgO, we find (using $q = \frac{1}{2}$) a random strain splitting $\bar{\delta} = 4.5$ cm^{-1}. A somewhat smaller value of 1.5 cm^{-1} was reported for Ru^{3+} in MgO.[37] We assume that the value of $\bar{\delta}$ in CaO will be of the same order as that in MgO. This assumption is based on results obtained for tetragonal spectra of Ir^{4+} in MgO and CaO.[20] Thus we obtain for the tunneling splitting $3\Gamma < 0.45$ cm^{-1}, for both crystals.

It is of interest to estimate the JT energy. Following Ham's[12] analysis we calculated the linear JT coupling coefficient V and the JT energy E_{JT}. For the effective mass μ we used the mass of a single oxygen atom. Since the octahedral complex surrounding the JT ion is actually coupled to a continuum of phonon vibrations one should use an effective frequency ω_{eff} instead of ω. We used the values $\omega_{\text{eff}} = 400$ cm^{-1} and $\omega_{\text{eff}} = 300$ cm^{-1} cited by Englman[13] and obtained 2230 and 1140 cm^{-1} for E_{JT} for MgO and CaO, respectively. The value of ρ_0 is about the same for both hosts (0.24 Å). From this the difference between the Ir^{2+}-O^{2-} bond lengths in the elongated octahedron were calculated to be $\frac{1}{2}\sqrt{3}\rho_0 \sim 0.21$ Å. The values of $E_{JT}/\hbar\omega$ are 5.6 and 3.8 for MgO and CaO, respectively. The relatively large JT couplings ($E_{JT}/\hbar\omega > 1$) obtained here are consistent with the large radial extent of the 5d electron wave functions. For $E_{JT}/\hbar\omega \gtrsim 1$ the rotational kinetic energy is given quite accurately[12] as $\alpha = \hbar\omega(4E_{JT}/\hbar\omega)^{-1}$. For $E_{JT}/\hbar\omega \gtrsim 2$ the nonlinear JT coupling coefficient β and the energy splitting Δ between the first excited vibronic singlet A_1 and the next lowest singlet A_2 can be found from graphs given by Williams *et al.*[38] We obtain for MgO: $\beta > 370$ cm^{-1}, $\Delta > 280$ cm^{-1}; and for CaO: $\beta > 420$ cm^{-1}, $\Delta > 320$ cm^{-1}.

As pointed out in Sec. IV, the temperature range T_t at which the transition from the low-temperature anisotropic spectrum to the high-temperature isotropic spectrum of Ir^{2+} occurs is relatively high, which is consistent with a strong vibronic coupling. T_t is in the range 120–170 K and 160–180 K for MgO and CaO, respectively. Thus at 4.2 K the vibronic singlet A_2 is not populated, which is consistent with our large value of Δ, nor can motional averaging occur, which again means that $\tau\Delta\omega_L \gg 1$. τ^{-1} is the rate of the motional averaging (as pointed out in Sec. IV), and $\Delta\omega_L$ is the Larmor frequency difference between the corresponding resonance lines for the different distorted configurations. With H_{dc} along the [100] direction at $g_{[111]}$ we get $\Delta\omega_L = 2\pi\nu(g_\perp - g_\parallel)/g_{[111]}$, where ν is the klystron frequency. Taking $\nu = 9.4$ GHz, we obtain $\Delta\omega_L = 12.5\times 10^9$ sec^{-1} and 17.5×10^9 sec^{-1} for MgO and CaO, respectively. At low temperatures, the direct relaxation process is dominant, and one obtains for τ^{-1},[13]

$$\tau^{-1} = \frac{(qV_s)^2(3\Gamma)^2\frac{3}{2}\bar{\delta}}{5\pi d\hbar^4 v_T^5}\left[1+\frac{2}{3}\left(\frac{v_T}{v_L}\right)^5\right]\left(\frac{e^{3\bar{\delta}/2kT}+2}{e^{3\bar{\delta}/2kT}-1}\right).$$

Here d, v_T, and v_L are the specific density, the transverse and longitudinal sound velocity, respectively. We used, for MgO,[39] $d = 3.58$ g/cm^3, $v_T = 6.6\times 10^5$ cm/sec, $v_L = 9.1\times 10^5$ cm/sec, and for CaO,[40] $d = 3.3$ g/cm^3, $v_T = 4.8\times 10^5$ cm/sec, $v_L = 7.8\times 10^5$ cm/sec, and obtained $\tau > 27\times 10^{-9}$ sec and $\tau > 14\times 10^{-9}$ sec, for Ir^{2+} in MgO and CaO, respectively. Thus at 4.2 K for both crystals $\tau\Delta\omega_L \gg 1$ (of the order of 10^2), and there is no motional averaging at this temperature. At high temperatures where the Raman and/or Orbach processes are dominant, the relaxation rate becomes much greater, satisfying the condition for motional averaging. Since Δ is of the order of 300 cm^{-1}, the population of the excited singlet A_2 at 200 K will be approximately 10%. Thus the main contribution to the high-temperature isotropic spectrum is in our case due to motional averaging.

The variation of the linewidth of the isotropic spectrum in MgO as a function of temperature and direction of the magnetic field with respect to the crystalline axes can be explained qualitatively by a combination of two relaxation mechanisms. One relaxation mechanism is due to motional averaging ($\Delta\omega_L^2\tau$) and causes the linewidth to decrease with increasing temperature. The contribution of the motional averaging to the linewidth is also dependent on the direction of the external magnetic field H_{dc}, i.e., it is zero with H_{dc} along the [111] direction and maximum with H_{dc} along the [100] direction. The other mechanism is due to spin-lattice relaxation effects and causes an increase in linewidth with increasing temperature. At high tem-

peratures where the mechanism of spin-lattice relaxation effects is dominant, an isotropic linewidth is obtained. The superposition of these two relaxation mechanisms causes a minimum in the linewidth versus temperature relationship (except in the [111] direction, where the contribution to the motional averaging vanishes).

VI. SUMMARY

The EPR spectrum of Ir^{2+} in MgO and CaO exhibits a static JT effect and a strong QI. From the narrow linewidths at low temperatures, symmetrical line shapes, and the angular variation of the spectrum, we conclude that in both hosts, $\bar{\delta}/3\Gamma > 10$. Thus we are concerned here with a "pure" static JT effect. Very little or no strain broadening is also consistent with our results, i.e., that we were not able to observe coexistence of the isotropic and anisotropic spectrum. Since $g_{\parallel} < g_{\perp}$, it follows for a d^7 low-spin configuration that the first excited vibronic level is a singlet A_1 and that V and β, the linear and nonlinear JT coupling coefficients, respectively, are positive. The values of the calculated parameters of the vibronic Hamiltonian given in Table II are consistent with a static JT effect. Large values of the energy splitting Δ, between the first excited vibronic singlet A_1 and the next lowest singlet A_2, indicate that the high-temperature spectrum is mainly due to motional averaging. This is further supported for MgO by an observed minimum in the variation of the linewidth of the isotropic spectrum as a function of temperature in the [100] direction. The unusually high T_t values (the temperature at which the transition from the high to the low-temperature spectrum occurs) are consistent with the assumed strong JT coupling, which again results in a small tunneling splitting 3Γ. The high T_t are also consistent with the relatively large g-shifts Δg (where $\Delta g = g_{\perp} - g_{\parallel}$).

The electric field gradient required for the QI is in our case caused by the JT distortion. The QI was found to be strong in both cases; in MgO it is much larger than the hyperfine interaction ($Q/A_{\perp} \sim 2$), and in CaO it is smaller ($Q/A_{\perp} \sim 0.25$). The anomalous effects in the EPR spectra of Ir^{2+} in MgO and CaO, caused by the strong QI, were interpreted by an exact diagonalization of the spin Hamiltonian. The differences in g values between MgO and CaO were found consistent with the different crystal-field strengths of these hosts.

ACKNOWLEDGMENTS

The MgO crystals used in this study were grown by the late Max Foguel. We are grateful to Dr. N. V. Vugman for sending us the Fortran IV version of the MAGNSPEC program and his Ph.D. thesis, as well as for helpful correspondence. Useful discussions with Dr. A. Zussman are gratefully acknowledged.

---

*This work represents part of a Ph.D. thesis submitted by A. Raizman to Tel-Aviv University.

[1]A. Abragam and B. Bleaney, *Electron Paramagnetic Resonance of Transition Metal Ions* (Oxford U.P., Oxford, England, 1970).

[2]N. V. Vugman, A. O. Caride, and J. Danon, J. Chem. Phys. 59, 4418 (1973).

[3]H. Van Willigen and J. G. M. Van Rens, Chem. Phys. Lett. 2, 283 (1968).

[4]J. C. Danner, U. Ranon, and D. N. Stamires, Phys. Rev. B 3, 2141 (1971).

[5]Chien-Chung Chao and Jack H. Lunsford, J. Chem. Phys. 59, 3920 (1973).

[6]R. H. Borcherts, H. Kanzaki, and M. Abe, Phys. Rev. B 2, 23 (1970).

[7]J. R. Herrington, T. L. Estle, and L. A. Boatner, Phys. Rev. B 5, 2500 (1972).

[8]A. O. Barksdale, Ph.D. thesis (Rice University, 1973) (unpublished).

[9]F. W. Webster and R. A. D. White, J. Cryst. Growth 5, 167 (1969).

[10]J. M. Mackey, M. Kopp, E. C. Tynan, and Teh Fu Yen, in *ESR of Metal Complexes*, edited by Teh Fu Yen (Plenum, New York, 1969), p. 33.

[11]M. D. Sturge, in *Solid State Physics*, edited by F. Seitz and D. Turnbull (Academic, New York, 1967), Vol. 20, p. 91.

[12]F. S. Ham, in *Electron Paramagnetic Resonance*, edited by S. Geschwind (Plenum, New York, 1972), p. 1; F. S. Ham, Phys. Rev. B 11, 3854 (1971).

[13]R. Englman, *The Jahn-Teller Effect in Molecules and Crystals* (Wiley, New York, 1972).

[14]R. W. Reynolds and L. A. Boatner, Phys. Rev. B 12, 4735 (1975).

[15]S. Sugano, Y. Tanabe, and H. Kamimura, *Multiplets of Transition Metal Ions in Crystals* (Academic, New York, 1970).

[16]A. Narath, Phys. Rev. 165, 506 (1968).

[17]W. J. Childs, M. Fred, E. Schrodl, and Th. A. M. van Kleef, Phys. Rev. A 10, 1028 (1974).

[18]In designating the resonance lines as a_i, b_i, c_i, and d_i ($i = 0$, 1, or 2), in most figures no distinction was made between isotope 191 and 193. Wherever the distance between the lines is large the letters were placed above the lines due to isotope 193.

[19]J. T. Suss, W. Low, and M. Foguel, Phys. Lett. A 33, 14 (1970).

[20]A. Raizman, Ph.D. thesis (Tel-Aviv University, 1976) (unpublished).

[21]N. V. Vugman, R. P. A. Muniz, and D. Danon, J.

Chem. Phys. 57, 1297 (1972).
[22]A. Raizman, A. Schoenberg, J. T. Suss, and S. Szapiro, Bull. Israel Phys. Soc., 1974 (unpublished), p. 64.
[23]E. Šimánek, Z. Šroubek, K. Ždánský, J. Kaczér, and I. Novák, Phys. Status Solidi 14, 333 (1966).
[24]J. A. Hodges, R. A. Serway, and S. A. Marshall, Phys. Rev. 151, 196 (1966).
[25]S. Geschwind and J. P. Remeika, J. Appl. Phys. 33, 370 (1962).
[26]J. T. Suss, A. Raizman, S. Szapiro, and W. Low, J. Magn. Resonance 6, 438 (1972).
[27]A. Raizman and J. T. Suss, in *Proceedings of the Eighteenth Ampere Congress on Magnetic Resonance and Related Phenomena, Nothingham, 1974,* edited by P. S. Allen, E. R. Andrew, and C. A. Bates (unpublished), Vol. I, p. 121.
[28]A. Schoenberg, J. T. Suss, Z. Luz, and W. Low, Phys. Rev. B 9, 2047 (1974).
[29]W. Low and J. T. Suss, Phys. Lett. 7, 310 (1963); U. Höchli, K. A. Müller, and P. Wysling, Phys. Lett. 15, 5 (1965).
[30]R. Lacroix, U. Höchli, and K. A. Müller, Helv. Phys. Acta 37, 627 (1964).
[31]Y. Tanabe and S. Sugano, J. Phys. Soc. Jpn. 9, 753 (1954).
[32]C. K. Jørgensen, *Absorption Spectra and Chemical Bonding in Complexes* (Pergamon, New York, 1962), Chap. 7.
[33]L. W. Panek and G. T. Perlow, Report No. ANL-7631, Argonne National Laboratory, Argonne, Ill. (unpublished).
[34]A. J. Freeman, J. V. Mallow, and P. S. Bagus, J. Appl. Phys. 41, 1321 (1970).
[35]T. Krigas and M. T. Rogers, J. Chem. Phys. 55, 3035 (1971), and references therein.
[36]A. M. Stoneham, Proc. Phys. Soc. Lond. 89, 909 (1966).
[37]A. Raizman, J. T. Suss, and S. Szapiro, Solid State Commun. 9, 1799 (1971).
[38]F. I. B. Williams, D. C. Krupka, and D. P. Breen, Phys. Rev. 179, 225 (1969).
[39]G. R. Barsch and Z. P. Chang, Phys. Status Solidi 19, 139 (1967).
[40]H. E. Hite and R. J. Kearney, J. Appl. Phys. 38, 5424 (1967).